Available online at www.sciencedirect.com

SciVerse ScienceDirect

Ceramics International 39 (2013) 8059–8063

CERAMICS INTERNATIONAL

www.elsevier.com/locate/ceramint

Photocatalytic hydrogen production over In_2S_3–Pt–$Na_2Ti_3O_7$ nanotube films under visible light irradiation

Jiawen Liu[a,*], Tao Ding[a], Zhonghua Li[b,**], Jingxiang Zhao[a], Shuying Li[a], Jihong Liu[a]

[a] Key Laboratory for Photonic and Electronic Bandgap Materials, Ministry of Education, and College of Chemistry and Chemical Engineering, Harbin Normal University, Harbin 150025, PR China

[b] Key Laboratory of Microsystems and Microstructures Manufacturing, Ministry of Education, Harbin Institute of Technology, Harbin 150001, PR China

Received 29 December 2012; received in revised form 28 February 2013; accepted 24 March 2013
Available online 3 April 2013

Abstract

$Na_2Ti_3O_7$ nanotube films were prepared by hydrothermal treatment of Ti foils in NaOH solution. Pt and In_2S_3 were effectively deposited on the surface of the $Na_2Ti_3O_7$ nanotube films by photochemical reduction and precipitation reaction, respectively. The prepared samples were characterized by X-ray diffraction (XRD), scanning electron microscopy (SEM), X-ray photoelectron spectroscopy (XPS) and UV–vis diffuse reflectance spectroscopy (DRS). The results of XRD, XPS and SEM indicate that In_2S_3 is coupled on the surface of $Na_2Ti_3O_7$ nanotube films. Compared with $Na_2Ti_3O_7$ nanotube film, the absorption edges of In_2S_3–$Na_2Ti_3O_7$ nanotube films are extended to the visible region, which lead to the visible light photocatalytic hydrogen production activities of In_2S_3–$Na_2Ti_3O_7$ nanotube films. The experiment results show that the ternary hybrid In_2S_3–Pt–$Na_2Ti_3O_7$ nanotube thin films possess much higher photocatalytic activities than In_2S_3–$Na_2Ti_3O_7$ nanotube thin films. Moreover, the mechanism of photocatalysis over In_2S_3–Pt–$Na_2Ti_3O_7$ nanotubes under visible light was discussed.

Keywords: $Na_2Ti_3O_7$ nanotube films; Visible light; Photocatalysis; Hydrogen production

1. Introduction

The rapid depletion of fossil fuels and the pollution problems associated with their use urgently require the development of alternative, sustainable and environmentally friendly energy sources. Hydrogen has been identified as an ideal energy carrier due to its clean, storable and renewable properties. Photocatalytic splitting of water into hydrogen over semiconductors is regarded as one of the most attractive way to produce hydrogen. Hence, the nanostructured semiconductor photocatalysts were widely developed and researched, such as titanate nanotubes [1–4], TiO_2 nanowires [5,6], TiO_2 nanofibers [7,8] and nanosized $NaTaO_3$ [9,10] have been widely developed due to their unique structures and attractive potential applications. Especially, nanotube photocatalysts exhibit desirable properties for their applications in solar energy conversion due to their high specific surface area and controllable morphology [11–15]. However, most of them only respond to UV light irradiation because of their wide band gap. In recent years, considerable effort has been made to extend their absorption into visible light. Coupling with narrow band gap semiconductors, such as CdS [16–18], Bi_2S_3 [19,20], In_2S_3 [21,22] and Cu_2O [23,24], is an effective method to improve the photocatalytic efficiency and extend the optical spectral response of a wide band gap semiconductor. Recently, ternary hybrid photocatalysts such as Pt–CdS–TiO_2 [25] and CdS–TiO_2–Au [26] have received much attention due to the further reduction of electron–hole pair recombination with the introduction of noble metal.

In the present study, In_2S_3–$Na_2Ti_3O_7$ nanotube thin films were successfully prepared. These films exhibit good photocatalytic activities for hydrogen production from Na_2S/Na_2SO_3 aqueous solution. The effects of $InCl_3$ concentration on photocatalytic activities of In_2S_3–$Na_2Ti_3O_7$ nanotube films were investigated. Moreover, the mechanism of photocatalytic activity enhancement of the three-component In_2S_3–Pt–$Na_2Ti_3O_7$ film was discussed in detail.

*Corresponding author. Tel.: +86 451 88060570; fax: +86 451 88060653.
**Corresponding author.
E-mail addresses: jiawenliu@yahoo.com.cn (J. Liu), lizh@hit.edu.cn (Z. Li).

0272-8842/$ - see front matter © 2013 Elsevier Ltd and Techna Group S.r.l. All rights reserved.
http://dx.doi.org/10.1016/j.ceramint.2013.03.077

2. Experiments

2.1. Sample preparation

In a typical fabrication process, Ti foils, $2.0 \times 3.0\ cm^2$, were ultrasonically cleaned in acetone and ethanol for 30 min. Then, the Ti foils were put into 30 ml Teflon-lined hydrothermal vessels with 20 ml of 10 M NaOH aqueous solution and heated at 140 °C for 12 h to form $Na_2Ti_3O_7$ nanotube films. In order to enhance the photocatalytic activities of the as-prepared $Na_2Ti_3O_7$ nanotube films, the noble metal Pt was loaded on the $Na_2Ti_3O_7$ nanotubes by the photochemical reduction method. $Na_2Ti_3O_7$ nanotube films were vacuumized at 60 °C for 10 min after 0.02 mL of 4 mM H_2PtCl_6 was spread on it. Then, the samples were irradiated with ultraviolet light in 40 mL methanol for 1 h to reduce Pt ions.

In_2S_3 nanoparticles were deposited by using the successive ionic layer adsorption and reaction (SILAR) method. $Na_2Ti_3O_7$ nanotube films or Pt loaded $Na_2Ti_3O_7$ nanotube films were immersed in $InCl_3$ solution for 10 min under vacuum conditions, and kept for 20 min after exhausting to get adsorbed In^{3+} ions, followed by drying in air. Then, the films were immersed in Na_2S solution for 10 min under vacuum condition, and kept for 20 min after exhausting to make S^{2-} ions react with In^{3+} ions. This SILAR cycles were repeated three times to obtain desired In_2S_3–$Na_2Ti_3O_7$ nanotube films or In_2S_3–Pt–$Na_2Ti_3O_7$ nanotube films.

2.2. Characterization

The morphologies of the prepared samples were obtained on a HITACHI S-4800 field emission scanning electron microscopy (FE-SEM). The crystalline phases were identified by X-ray diffraction (XRD) using a Rigaku D/MAX-RB diffractometer with Cu Kα radiation. The surface compositions and chemical states of elements in samples were investigated by X-ray photoelectron spectroscopy (XPS) on a PHI 5700 ESCA System with an Al Kα X-ray source. UV–vis diffuse reflection spectra (DRS) were recorded on a HITACHI U-4100 spectro-

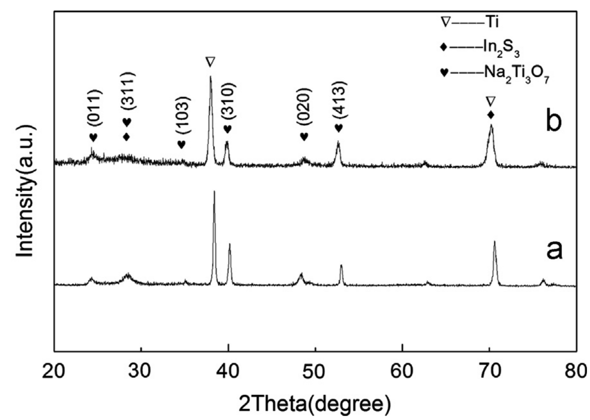

Fig. 2. XRD patterns of (a) $Na_2Ti_3O_7$ nanotube film and (b) In_2S_3–$Na_2Ti_3O_7$ nanotube film obtained in the presence of 0.1 M $InCl_3$.

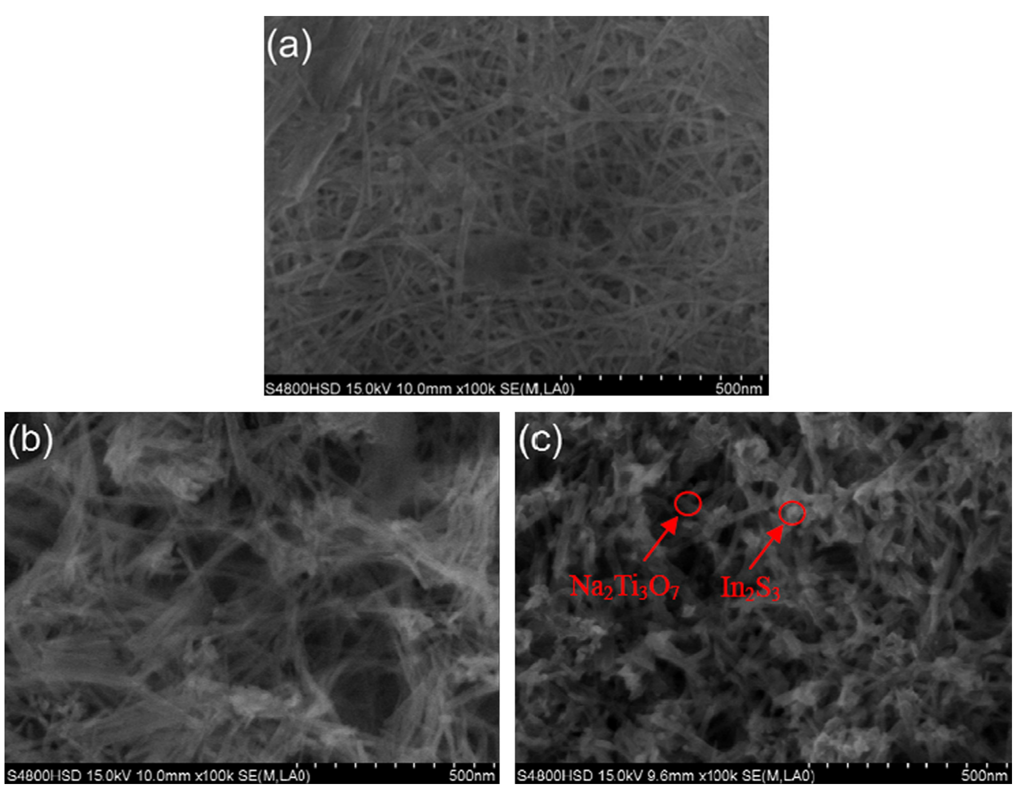

Fig. 1. SEM images of $Na_2Ti_3O_7$ nanotube film (a) and In_2S_3–$Na_2Ti_3O_7$ nanotube films obtained at different concentrations of $InCl_3$ (b) 0.05 M and (c) 0.1 M.

photometer, and were converted to absorbance spectra through the standard Kubelka–Munk method.

2.3. Photocatalytic activity

Photocatalytic hydrogen production measurements were carried out in a column quartz reactor. The prepared film was immersed in 50 mL mixed aqueous solution containing 0.3 M Na_2S and 0.2 M Na_2SO_3. The solution was irradiated by a 500 W high-pressure Xe lamp for 1 h. The distance between the light source and column reactor was 10 cm. Meanwhile, the reaction solution was stirred with a magnetic stirrer. The amount of generated hydrogen was measured by a gas chromatograph (thermal conductivity detector, molecular sieve 5 Å column, Ar carrier).

3. Results and discussion

3.1. Morphology measurement

SEM images of $Na_2Ti_3O_7$ nanotubes and In_2S_3–$Na_2Ti_3O_7$ nanotubes are shown in Fig. 1. From Fig. 1(a), it can be seen that $Na_2Ti_3O_7$ nanotubes can be successfully obtained with external diameters of ~10 nm at 140 °C as reported in our previous work [27]. Fig. 1(b) and (c) shows the SEM images of In_2S_3–$Na_2Ti_3O_7$. From Fig. 1(b) and (c), it can be clearly seen that $Na_2Ti_3O_7$ nanotubes are decorated with In_2S_3 without suffering morphological transformation. The average size of In_2S_3 nanoparticles is about 20 nm as shown in Fig. 1(c). Moreover, the amount of In_2S_3 increases with the increase of concentrations of $InCl_3$.

3.2. XRD patterns

Fig. 2(a) shows the XRD pattern of $Na_2Ti_3O_7$ nanotube film on Ti substrate. The main characteristic peaks can be well indexed to the cubic structure of perovskite $Na_2Ti_3O_7$ (JCPDS Card no. 31-1329). It indicates that the cubic $Na_2Ti_3O_7$ nanotubes have been successfully fabricated by hydrothermal treatment of Ti foil. Ti peaks can be found in Fig. 2 due to the low film thickness. The XRD pattern of In_2S_3–$Na_2Ti_3O_7$ nanotube film is shown in Fig. 2(b). Compared with Fig. 2 (a), it is found that the diffraction peaks of In_2S_3 are not obvious due to the very small content.

3.3. XPS analysis

To determine the chemical states of In_2S_3 species in the $In_2S_3/Na_2Ti_3O_7$ nanotube films, the XPS measurement of In_2S_3–$Na_2Ti_3O_7$ nanotube film was carried out. High resolution core spectrum for In 3d and S 2p is displayed in Fig. 3(a) and (b), respectively. The In 3d X-ray photoelectron spectrum consists of two peaks at 445.2 and 452.8 eV attributed to In $3d_{5/2}$ and In $3d_{3/2}$, respectively. The difference between the split orbit peaks is 7.6 eV. Only one component located at 161.9 eV for S 2p was detected for In_2S_3–$Na_2Ti_3O_7$ nanotube film. The values of In 3d and S 2p are in agreement with the binding energy usually reported for In_2S_3 [28–30]. These results indicate that the chemical states of In and S in the samples are In^{3+} and S^{2-} respectively.

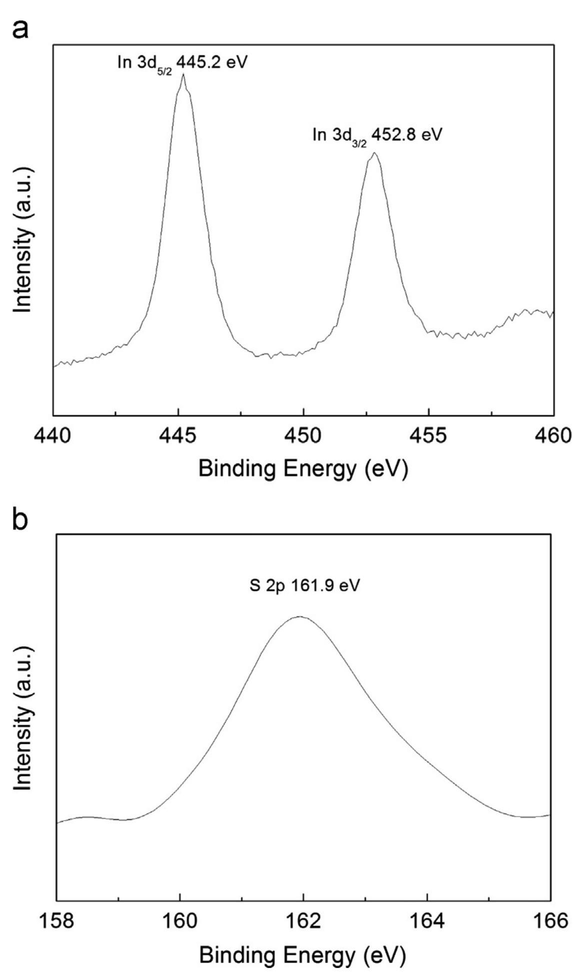

Fig. 3. XPS spectra of In_2S_3–$Na_2Ti_3O_7$ nanotube film: (a) In 3d and (b) S 2p.

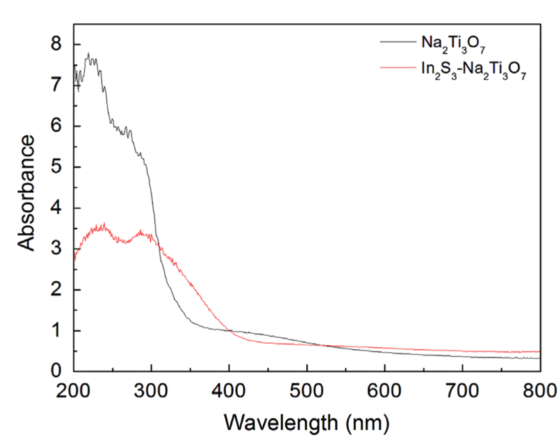

Fig. 4. Diffuse reflectance spectra of (a) $Na_2Ti_3O_7$ nanotube film and (b) In_2S_3–$Na_2Ti_3O_7$ nanotube film obtained in 0.1 M $InCl_3$.

3.4. DRS analysis

The UV–vis diffuse reflectance spectra of unmodified $Na_2Ti_3O_7$ and In_2S_3–$Na_2Ti_3O_7$ nanotube films are shown in Fig. 4. It can be seen that the absorption edge of the $Na_2Ti_3O_7$ nanotube film is located at 340 nm, whereas the absorption edge of the In_2S_3–$Na_2Ti_3O_7$ nanotube film is shifted to approximately 440 nm. The optical band gap energies calculated from the absorption edges are about 3.6 eV and 2.8 eV. This result indicates that the addition of In_2S_3 leads to a red-shift in composite photocatalysts, demonstrating that the absorption spectrum of $Na_2Ti_3O_7$ nanotubes can be extended into the visible light region by coupling with In_2S_3.

3.5. Photocatalytic activity and mechanism

The photocatalytic activities of In_2S_3–$Na_2Ti_3O_7$ and In_2S_3–Pt–$Na_2Ti_3O_7$ nanotube films are evaluated by photocatalytic H_2 production from Na_2S/Na_2SO_3 aqueous solution under visible light irradiation. Moreover, the effects of $InCl_3$ concentration on photocatalytic activities of In_2S_3–$Na_2Ti_3O_7$ nanotube films were investigated. Fig. 5 shows the hydrogen production rates of In_2S_3–$Na_2Ti_3O_7$ and In_2S_3–Pt–$Na_2Ti_3O_7$ nanotube films under visible light irradiation. The hydrogen production rate increases significantly with the increase of $InCl_3$ concentration from 0.05 to 0.1 M, and then decreases with the further increase of $InCl_3$ concentration. This is due to the sizes of In_2S_3 nanoparticles that increase with the increase of $InCl_3$ concentration. An optimum coverage of In_2S_3 nanoparticles decorating $Na_2Ti_3O_7$ nanotubes will contribute to an efficient electron–hole pairs separation and the electrons fast transport, and thus to enhance the photocatalytic activity. But excessive coverage of In_2S_3 nanoparticles on the surface of $Na_2Ti_3O_7$ nanotubes would reduce photocatalytic active sites for H_2 evolution and reduce the reaction probability of electrons and water molecule at the $Na_2Ti_3O_7$ surface, resulting in the decreasing of photocatalytic activity. Therefore, there is an optimum concentration of $InCl_3$ solution (0.1 M) for achieving high photocatalytic hydrogen production activity. In addition, compared with In_2S_3–$Na_2Ti_3O_7$ nanotube films, In_2S_3–Pt–$Na_2Ti_3O_7$ nanotube film shows an excellent photocatalytic performance. The enhancement of photocatalytic activity is attributed to the efficient charge separation in In_2S_3–Pt–$Na_2Ti_3O_7$ photocatalyst. The mechanism of charge transfer and separation in the three-component (3C) system is illustrated in Fig. 6.

For the In_2S_3–$Na_2Ti_3O_7$ nanotube film 2C system, the narrow band gap semiconductor In_2S_3 absorbs visible light and generates electrons and holes; the photoinduced electrons are injected from In_2S_3 into the conduction band of attached $Na_2Ti_3O_7$ nanotubes. Therefore, a better visible-light photocatalytic activity is obtained. However, the photocatalytic activity of the 2C system is far lower than that of the In_2S_3–Pt–$Na_2Ti_3O_7$ nanotube film 3C system. For the In_2S_3–Pt–$Na_2Ti_3O_7$ nanotube film 3C system, the photogenerated electrons that migrated from In_2S_3 to $Na_2Ti_3O_7$ nanotubes will immediately transfer to Pt. Electrons that arrived at Pt will react with H^+ to form H_2, resulting in an efficient separation of photogenerated charge carriers. Therefore, the photocatalytic activity of the In_2S_3–Pt–$Na_2Ti_3O_7$ nanotube film 3C system is improved by loading Pt compared with the In_2S_3–$Na_2Ti_3O_7$ nanotube film 2C system.

4. Conclusions

In_2S_3–$Na_2Ti_3O_7$ and In_2S_3–Pt–$Na_2Ti_3O_7$ nanotube films were successfully fabricated by combining the hydrothermal method, photochemistry reduction and SILAR method. The present results show that coupling of In_2S_3 significantly extends the photoresponse of the $Na_2Ti_3O_7$ nanotubes into the visible region. The as-prepared In_2S_3–$Na_2Ti_3O_7$ nanotube films are active as a photocatalyst under visible light irradiation. In_2S_3–Pt–$Na_2Ti_3O_7$ nanotube film has a much higher photocatalytic activity than that of In_2S_3–$Na_2Ti_3O_7$ nanotube film, indicating that Pt loading plays an important role in enhancing the photocatalytic activity of In_2S_3–$Na_2Ti_3O_7$ nanotube films.

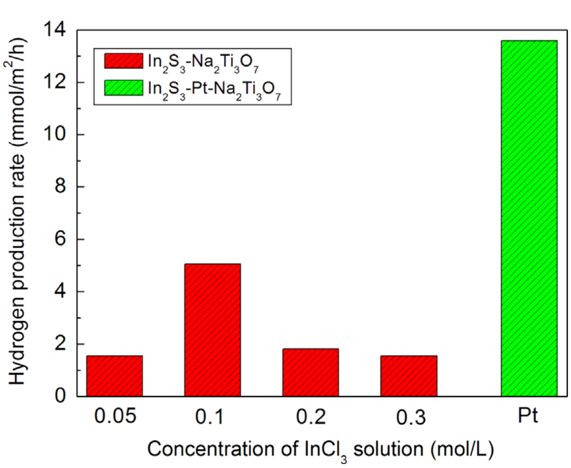

Fig. 5. Hydrogen generation rate of In_2S_3–$Na_2Ti_3O_7$ nanotube films obtained in different concentrations of $InCl_3$ solution and In_2S_3–Pt–$Na_2Ti_3O_7$ nanotube film obtained in 0.1 M $InCl_3$.

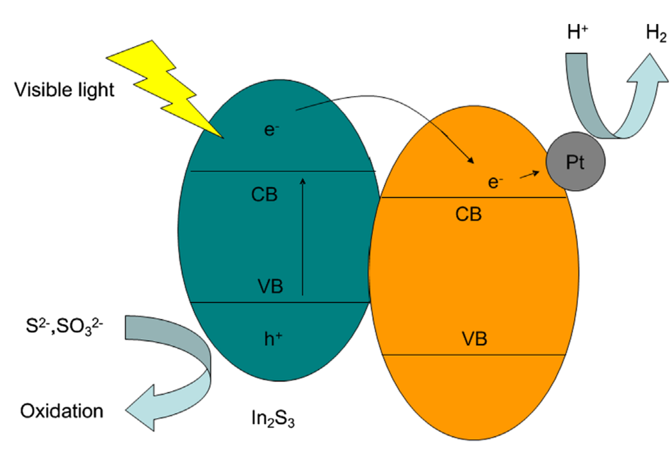

Fig. 6. Schematic representation of charge transfer of water photosplitting on the In_2S_3–Pt–$Na_2Ti_3O_7$ nanotube film. CB and VB refer to the energy levels of the conduction and valence bands, respectively.

Acknowledgments

This work was supported by Science Foundation of Educational Commission of Heilongjiang Province (11541096).

References

[1] V. Bem, M.C. Neves, M.R. Nunes, A.J. Silvestre, O.C. Monteiro, Influence of the sodium/proton replacement on the structural, morphological and photocatalytic properties of titanate nanotubes, Journal of Photochemistry and Photobiology A: Chemistry 232 (2012) 50–56.
[2] J. Yu, H. Yu, B. Cheng, C. Trapalis, Effects of calcination temperature on the microstructures and photocatalytic activity of titanate nanotubes, Journal of Molecular Catalysis A: Chemical 249 (2006) 135–142.
[3] J. Liu, Y. Sun, Z. Li, Ag loaded flower-like $BaTiO_3$ nanotube arrays: Fabrication and enhanced photocatalytic property, CrystEngComm 14 (2012) 1473–1478.
[4] J. Liu, Y. Sun, Z. Li, S. Li, J. Zhao, Photocatalytic hydrogen production from water/methanol solutions over highly ordered Ag–$SrTiO_3$ nanotube arrays, International Journal of Hydrogen Energy 36 (2011) 5811–5816.
[5] J. Jitputti, Y. Suzuki, S. Yoshikawa, Synthesis of TiO_2 nanowires and their photocatalytic activity for hydrogen evolution, Catalysis Communications 9 (2008) 1265–1271.
[6] N. Xiao, Z. Li, J. Liu, Y. Gao, A facile template-free method for preparing bi-phase TiO_2 nanowire arrays with high photocatalytic activity, Materials Letters 64 (2010) 1776–1778.
[7] M.S. Hassan, T. Amna, O.B. Yang, H.C. Kim, M.S. Khil, TiO_2 nanofibers doped with rare earth elements and their photocatalytic activity, Ceramics International 38 (2012) 5925–5930.
[8] R. Nirmala, H.Y. Kim, R. Navamathavan, C. Yi, J.J. Won, K. Jeon, A. Yousef, R. Afeesh, M. El-Newehy, Photocatalytic activities of electrospun tin oxide doped titanium dioxide nanofibers, Ceramics International 38 (2012) 4533–4540.
[9] X. Li, J. Zang, Hydrothermal synthesis and characterization of Lanthanum-doped $NaTaO_3$ with high photocatalytic activity, Catalysis Communications 12 (2011) 1380–1383.
[10] Y. He, Y. Zhu, N. Wu, Synthesis of nanosized $NaTaO_3$ in low temperature and its photocatalytic performance, Journal of Solid State Chemistry 177 (2004) 3868–3872.
[11] M. Adachi, Y. Murata, M. Harada, Y. Yoshikawa, Formation of titania nanotubes with high photo-catalytic activity, Chemistry Letters 29 (2000) 942–943.
[12] S.Z. Chu, S. Inoue, K. Wada, D. Li, H. Haneda, S. Awatsu, Highly porous (TiO_2–SiO_2–TeO_2)/Al_2O_3/TiO_2 composite nanostructures on glass with enhanced photocatalysis fabricated by anodization and sol−gel process, Journal of Physical Chemistry B 107 (2003) 6586–6589.
[13] H. Li, L. Cao, W. Liu, G. Su, B. Dong, Synthesis and investigation of TiO_2 nanotube arrays prepared by anodization and their photocatalytic activity, Ceramics International 38 (2012) 5791–5797.
[14] K. Shankar, G.K. Mor, H.E. Prakasam, S. Yoriya, M. Paulose, O.K. Varghese, C.A. Grimes, Highly-ordered TiO_2 nanotube arrays up to 220 μm in length: use in water photoelectrolysis and dye-sensitized solar cells, Nanotechnology 18 (2007) 065707.
[15] M. Paulose, K. Shankar, S. Yoriya, H.E. Prakasam, O.K. Varghese, G.K. Mor, T.A. Latempa, A. Fitzgerald, C.A. Grimes, Anodic growth of highly ordered TiO_2 nanotube arrays to 134 μm in length, Journal of Physical Chemistry B 110 (2006) 16179–16184.
[16] C. Xing, D. Jing, M. Liu, L. Guo, Photocatalytic hydrogen production over $Na_2Ti_2O_4(OH)_2$ nanotube sensitized by CdS nanoparticles, Materials Research Bulletin 44 (2009) 442–445.
[17] C. Li, J. Yuan, B. Han, L. Jiang, W. Shangguan, TiO_2 nanotubes incorporated with CdS for photocatalytic hydrogen production from splitting water under visible light irradiation, International Journal of Hydrogen Energy 35 (2010) 7073–7079.
[18] C.J. Lin, Y.H. Yu, Y.H. Liou, Free-standing TiO_2 nanotube array films sensitized with CdS as highly active solar light-driven photocatalysts, Applied Catalysis B: Environmental 93 (2009) 119–125.
[19] J. Kim, M. Kang, High photocatalytic hydrogen production over the band gap-tuned urchin-like Bi_2S_3-loaded TiO_2 composites system, International Journal of Hydrogen Energy 37 (2012) 8249–8256.
[20] R. Brahimi, Y. Bessekhouad, A. Bouguelia, M. Trari, Visible light induced hydrogen evolution over the heterosystem Bi_2S_3/TiO_2, Catalysis Today 122 (2007) 62–65.
[21] C. Gao, J. Li, Z. Shan, F. Huang, H. Shen, Preparation and visible-light photocatalytic activity of In_2S_3/TiO_2 composite, Materials Chemistry and Physics 122 (2010) 183–187.
[22] S. Shen, L. Guo, Structural, textural and photocatalytic properties of quantum-sized In_2S_3-sensitized Ti-MCM-41 prepared by ion-exchange and sulfidation methods, Journal of Solid State Chemistry 179 (2006) 2629–2635.
[23] Z. Li, J. Liu, D. Wang, Y. Gao, J. Shen, Cu_2O/Cu/TiO_2 nanotube ohmic heterojunction arrays with enhanced photocatalytic hydrogen production activity, International Journal of Hydrogen Energy 37 (2012) 6431–6437.
[24] S. Hu, F. Zhou, L. Wang, J. Zhang, Preparation of Cu_2O/CeO_2 heterojunction photocatalyst for the degradation of Acid Orange 7 under visible light irradiation, Catalysis Communications 12 (2011) 794–797.
[25] N. Strataki, M. Antoniadou, V. Dracopoulos, P. Lianos, Visible-light photocatalytic hydrogen production from ethanol–water mixtures using a Pt–CdS–TiO_2 photocatalyst, Catalysis Today 151 (2010) 53–57.
[26] T. Lv, L. Pan, X. Liu, Z. Sun, Visible-light photocatalytic degradation of methyl orange by CdS–TiO_2–Au composites synthesized via microwave-assisted reaction, Electrochimica Acta 83 (2012) 216–220.
[27] N. Xiao, Z. Li, J. Liu, Y. Gao, Effects of calcination temperature on the morphology, structure and photocatalytic activity of titanate nanotube thin films, Thin Solid Films 519 (2010) 541–548.
[28] W. Qiu, M. Xu, X. Yang, F. Chen, Y. Nan, J. Zhang, H. Iwai, H. Chen, Biomolecule-assisted hydrothermal synthesis of In_2S_3 porous films and enhanced photocatalytic properties, Journal of Materials Chemistry 21 (2011) 13327–13333.
[29] X. Fu, X. Wang, Z. Chen, Z. Zhang, Z. Li, D.Y.C. Leung, L. Wu, X. Fu, Photocatalytic performance of tetragonal and cubic β-In_2S_3 for the water splitting under visible light irradiation, Applied Catalysis B: Environmental 95 (2010) 393–399.
[30] M.A. Franzman, R.L. Brutchey, Solution-phase synthesis of well-defined indium sulfide nanorods, Chemistry of Materials 21 (2009) 1790–1792.